Available online at www.sciencedirect.com
ScienceDirect
Journal of Catalysis 247 (2007) 51–60
JOURNAL OF CATALYSIS
www.elsevier.com/locate/jcat

On the mechanism of zirconia textural stabilization by siliceous species during digestion under basic conditions

N. Nahas [a], P. Afanasiev [a,*], C. Geantet [a], M. Vrinat [a], F. Wiss [b], S. Dahar [c]

[a] *Institut de Recherches sur la Catalyse, 2 avenue A. Einstein, 69626 Villeurbanne cedex, France*
[b] *Saint Gobain ZirPro, CREE, 550 avenue A. Jauffret, BP 224, 84306 Cavaillon cedex, France*
[c] *Saint Gobain NorPro, 3840 Fishcreek Road, Stow, OH 44224, USA*

Received 18 September 2006; revised 22 November 2006; accepted 17 January 2007

Available online 14 February 2007

Abstract

The mechanism of zirconia textural stabilization by means of basic reflux was studied. In agreement with earlier studies, zirconia was modified by silicon extracted from the glass material in the same manner as if silicon compounds (e.g., TEOS, SiO_2) had been added to the reaction mixtures. The reflux in a Teflon bulb without the addition of silicon did not lead to improved textural properties. EXAFS study of both refluxed and nonrefluxed specimens showed their similarity and probably some dehydration of the precipitate. The FTIR, NMR, and XPS spectroscopic characterizations suggested that silicon was strongly segregated on the surface, probably in the form of silicate moieties anchored on zirconia. A reflux stage was necessary to achieve efficient spreading of the silicate over the surface of the precipitate. For the solids calcined at 1173 K, the surface stabilization corresponded to the formation of a "metastable monolayer" coverage, similar to that observed for zirconias doped by other oxoanions, such as molybdate or tungstate. Isooctane hydrocracking and *o*-xylene hydrogenation were studied in the presence of Pt supported on the oxides as prepared. Hydrodesulfurization of thiophene was carried out in the presence of Mo and NiMo sulphides using the same supports. In all three reactions studied, the digested zirconia support demonstrated properties similar to those of pure silica.

Keywords: Zirconia; Silicate; Textural stabilization; Support effects; X-ray photoelectron spectroscopy; TEM

1. Introduction

Zirconium oxide is a promising support for various catalytic applications, including hydrotreating [1], partial oxidation [2], hydrogen production [3,4], and others. The textural properties of catalytic supports, such as specific surface area and pore volume, as well as their thermal stability, are of primary importance for these applications. To obtain zirconia supports with advantageous morphology, different preparation techniques have been proposed, including sol–gel [5], aerogel [6,7], molten salt [8,9] and surfactant-assisted [10,11] syntheses. Although all of these methods were more or less successful for doped zirconias, no pure ZrO_2 support with textural properties comparable to those of silica or alumina was obtained.

Earlier, Chuah et al. [12–14] found that the reflux of hydrous zirconia at basic pH led to a significant improvement in textural properties, increasing the specific surface area from ca. 100 m^2/g for the nondigested precipitates to >300 m^2/g for the digested precipitates. At the same time, excellent thermal stability was observed. This finding represented a real breakthrough in the preparation of zirconia catalytic supports. The effect was explained by coarsening of the hydrous zirconia network. The preparations were optimized in terms of concerns regarding the reflux pH and its duration, but various authors found very different values of textural parameters and optimal reflux conditions.

The problem was resolved recently when it was demonstrated that this texture-stabilizing effect was due to the silicon species coming from the glass vessels used for the reflux [15,16]. Therefore, the supports as prepared are not pure zirconias, but rather are doped with silicon. Thus, both the outstanding texture-improving effect and its poor reproducibility were explained. Questions remained, however, about the nature of

* Corresponding author.
E-mail address: afanas@catalyse.cnrs.fr (P. Afanasiev).

0021-9517/$ – see front matter
doi:10.1016/j.jcat.2007.01.009

this effect. Indeed, silica-doped zirconias obtained from various co-precipitation techniques are well known [17–22]. However, such a low silica content as that in digested solids never led to such strong textural stabilization effects. This paper deals with the elucidation of the silicon effect by characterization of digested zirconia and their comparison with silica-doped ZrO_2 specimens prepared by other techniques. The main question was whether the silicon species are completely located at the surface or are more or less homogeneously distributed between the surface and the bulk of such materials. The answer is important for catalytic applications of such supports; if high numbers of silicon species are located at the surface, then the corresponding catalytic supports should demonstrate silica-like behavior; otherwise they could be considered from a catalytic standpoint as doped zirconias.

2. Experimental

2.1. Support preparation

The solids were prepared by aqueous precipitation of zirconium oxychloride (Sigma) by an excess of aqueous ammonia, followed by different treatments. For the nonrefluxed specimens, the precipitate was filtered, thoroughly washed with distilled water, and oven-dried. Alternatively, the precipitates were then treated by reflux at pH 11 and 373 K in Teflon or glass vessels, or dried and impregnated with TEOS (Aldrich). The solids designations and preparation conditions are summarized in Table 1.

Calcination was carried out in flowing dry air (100 ml/min) for ca. 0.5 solids. Unless stated otherwise, the heating rate was 4 K/min, and the calcination time at final temperature was 2 h.

2.2. Catalyst preparation

Supported platinum catalysts (1% Pt) were prepared by incipient wetness impregnation using chloroplatinic acid (Sigma) as the metal precursor. The samples were calcined at 773 K for 2 h, then reduced under hydrogen at 573 K for 6 h. Other supports were used for comparison, γ alumina (Condea), silica (Grace), and silica-alumina (Condea; 40% of SiO_2; so-called SiAl40). A solution of the desired amount of hexachloroplatinic acid (H_2PtCl_6) in deionized water was added to the support. The amount of liquid required to fill the pore volume of the supports was about 0.3 ml/g for zirconia, 0.5 ml/g for alumina, and 1.4 ml/g for silica–alumina.

Table 1
Solid designations and preparation conditions

Reference	Preparation	Si content (wt%)
ZR-Reflux0	Precipitation, washing, and drying	–
ZR-Reflux72-Tefl	Precipitation, reflux 72 h at pH 11 in a Teflon bulb, washing, and drying	–
ZR-Reflux8	Precipitation, reflux 8 h at pH 11 in a glass bulb, washing, and drying	0.8
ZR-Reflux72	Precipitation, reflux 72 h at pH 11 in a glass bulb, washing, and drying	4.1
ZR-TEOS-Coprec	Co-precipitation of TEOS and ZOC, washing, and drying	1.6
ZR-TEOS-Reflux72	Co-precipitation of TEOS and ZOC, reflux 72 h in a Teflon bulb, washing, and drying.	1.6
ZR-TEOS-Imp	Impregnation of ZR-Reflux0 by TEOS, maturation 8 h, and drying	2.4

Supported Mo oxides were also obtained by the incipient wetness impregnation with ammonium heptamolybdate aqueous solutions, followed by drying and calcination at 723 K in air for 2 h, to decompose the precursor salts. The loading of metals was of 9 wt% Mo. Sulfidation of supported Mo oxides was carried out at a 3 h^{-1} weight flow of 15% H_2S–H_2 mixture, for 4 h at 673 K. The nonpromoted catalysts presulfided as described above were further handled under inert atmosphere. Then these supported sulfide Mo catalysts were impregnated with acetone solutions of the promoter salt $[Ni(NO_3)_2{\cdot}6H_2O]$ to obtain the 3 wt% loading of Ni calculated for the dried oxide catalyst. The catalysts were dried under nitrogen and resulfided for 1 h at 673 K in a H_2S–H_2 mixture.

2.3. Physicochemical characterizations

Chemical analyses were carried out by an atomic emission method using a Spectroflame ICP apparatus. Surface areas and pore size distributions were obtained by adsorption–desorption of N_2 at 77 K. Before measurements, all samples were evacuated at 673 K for 2 h. Calculations were done using BET and BJH equations. The X-ray diffraction (XRD) patterns were recorded on a Siemens D5005 diffractometer using Ni-filtered CuK_α radiation. The diffractograms were analyzed using the standard JCPDS files. ^{29}Si MAS NMR data were collected with a 400-MHz multinuclear FFT Bruker spectrometer at a Larmor frequency of 79.46 MHz. IR spectra were recorded with a Bruker Vector 22 spectrometer by using autosupported pellets of the solids in the IR cells with CaF_2 windows. Before the measurements, the pellets were evacuated at room temperature under dynamic pressure 0.01 Pa. High-resolution transmission electron microscopy (HRTEM) was done on a JEOL 2010 device, using a 200-kV accelerating voltage. X-ray photoelectron spectroscopy (XPS) analyses were performed using an ESCALAB 200R (VG Scientific) spectrometer with an AlK_α source (1486.6 eV). Platinum dispersion in the supported catalysts was measured by a hydrogen chemisorption technique.

EXAFS measurements were carried out at the European Synchrotron Radiation Facility (ESRF) in Grenoble on beamline FAME equipped with a Si(111) double-crystal monochromator. The samples were diluted with cellulose and pressed into a pellet. The EXAFS spectra were recorded at the Zr K-edge at room temperature, in transmission mode. The energy was calibrated using a Zr metal foil. The EXAFS data were treated with FEFF [23] and VIPER [24] programs. Then edge background was extracted using Bayesian smoothing with variable number of knots. The curve fitting was done alternatively in

the R and k spaces, and the fit was accepted only in the case of simultaneous convergence in k- and R-spaces (absolute and imaginary parts for the latter). Coordination numbers (CN), interatomic distances (R), Debye–Waller parameters (σ^2), and energy shifts (ΔE_0) were used as fitting variables. Constraints were introduced, relating the fitting parameters to get values lying in physically reasonable intervals. The quality of the fit was evaluated using the values of variance and goodness. Comparison between the models depending on different number of parameters was performed on the basis of F-test included in the VIPER software [24].

2.4. Catalytic tests

All of the experiments were carried out in catalytic microreactors operated in dynamic mode in the gas phase. Reactants were introduced by means of a gas saturator. Hydrogenating properties of the Pt catalysts were determined by structure-insensitive hydrogenation of *ortho*-xylene (1,2-dimethylbenzene). The reaction was carried out at 573 K and atmospheric pressure, with an *ortho*-xylene partial pressure of 4 kPa, a hydrogen flow rate of 0.45 ml/s, and a catalyst weight of 0.05–0.10 g.

Catalyst acidity was evaluated by hydrocracking (HC) of 2,2,4-trimethylpentane (isooctane) [25–27]. The reaction was carried out at 523 K and atmospheric pressure, with an isooctane partial pressure of 1.7 kPa, a hydrogen flow rate of 0.67 ml/s, and a catalyst weight of 0.05–0.15 g. Thiophene hydrodesulfurization (HDS) was carried out at 573 K and atmospheric pressure, with a thiophene partial pressure of 2.4 kPa and 100 kPa of hydrogen, a total flow rate of 6 l/h, and a catalyst weight of ca 0.1 g.

In all catalytic tests, the products were analyzed by gas chromatography. The specific rate was calculated in the steady state according to the equation $R = FX/m$, where R is the specific rate (mol/(g s)), F is molar flow rate of the reactant (mol/s), X is the conversion of reactant (kept below 20%), and m is the catalyst weight (g). The relative error on rate measurements was about 10%. The results of catalytic tests for different supports were compared at the same levels of conversion.

3. Results and discussion

The beneficial effect of silicon on zirconia textural properties was evaluated for different modes of silicon introduction. It appears that the same effect can be obtained whether the source of silicon is TEOS, dispersed silica, or the walls of glass bulbs used for reflux. Fig. 1 shows the surface areas of the samples calcined at 823 and 1173 K. The points corresponding to different modes of silicon introduction follow the same trend of increased surface area versus silicon content. At the same time, refluxed samples show considerably higher surface areas compared with their nonrefluxed counterparts, in which silicon was introduced by impregnation or co-precipitation. Therefore, refluxing treatment seems to be an important step for increasing the efficiency of silicon spreading and the textural stabilization of zirconia.

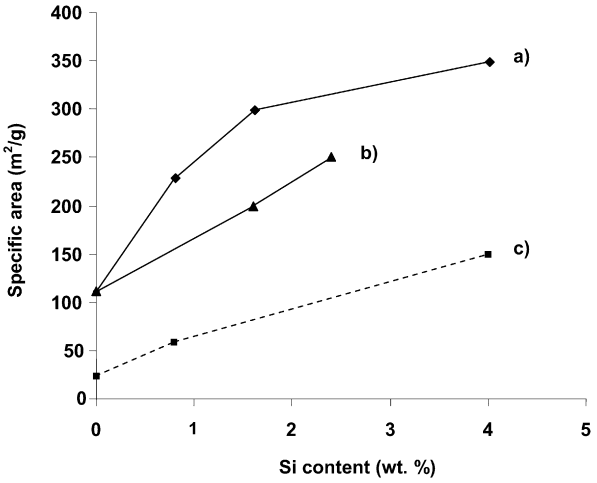

Fig. 1. Effect of the silicon content and the refluxing treatment on the specific surface area: (a) with reflux and calcination at 823 K for 2 h; (b) without reflux and calcination at 823 K for 2 h; (c) with reflux and calcination at 1173 K for 2 h.

Note that silicate moieties are stable in aqueous medium at the pH of refluxing treatment. As with refluxing in a Teflon bulb, this did not improve the textural properties for the calcination conditions that we applied. However, the effect of digestion itself cannot be dismissed on the basis of our study, which deals with only short calcination times. Indeed, digestion surely modifies the precipitate structure. Thus, according to our unpublished SANS data, it changes the fractal dimension of the precipitates at different Q vector scales (digestion increases it at short scales and decreases at long scales). Such changes likely will result in variations of longer time-sintering kinetics. A detailed investigation of sintering kinetics might be a subject of another study, but is beyond of scope of this paper.

3.1. Comparison of the dried solids

Although the influence of silicon was demonstrated to be the most probable reason of zirconia textural stabilization on digestion, speculations are still often met in the literature about the important changes due to basic digestion itself, independently of silicon incorporation [28,29]. There is nothing implausible in such assumption, because the texture-improving effects of aging are well known for silicas. To check whether the coordination of zirconium species was modified due to basic reflux, and whether this structure has common features with crystalline zirconia, we performed EXAFS study on the most relevant specimens: refluxed and nonrefluxed xerogels. It has been found that all the hydrous zirconia samples, whether initial or refluxed for 72 h, are X-ray-amorphous. Therefore, to follow the evolution of zirconium coordination, and the eventual differences between the solids, EXAFS spectra were recorded for dry precipitates obtained without reflux and after 72 h of reflux. The spectra were compared with the monoclinic zirconia reference.

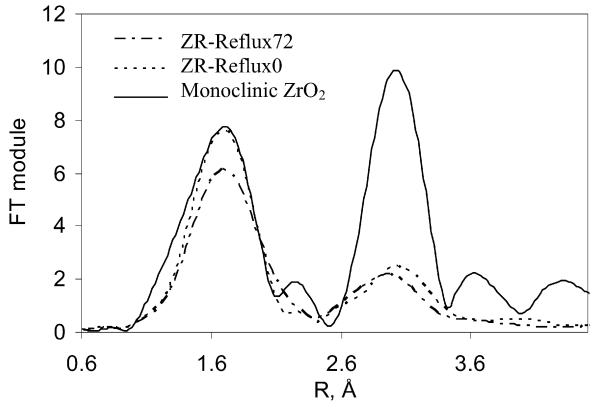

Fig. 2. Fourier transforms of the χk^3 EXAFS spectra of the digested precipitate, the nondigested precipitate and monoclinic zirconia reference.

The corresponding Fourier transform spectra are presented in Fig. 2. As can be seen, the general features of the FT spectra are similar for both amorphous solids prepared either with or without reflux. The amorphous solids show a much smaller contribution of the second neighbor, probably because both solids are strongly disorganized compared with the crystalline reference. No formation of "monoclinic-like" or "tetragonal-like" structures can be inferred from the EXAFS spectra, which in both cases would imply a strong increase of the second neighbor peak. As the only difference, some slight decrease in oxygen coordination number in the first shell was observed after reflux, as if some increase of the solid dispersion had occurred (Table 2). In general, the EXAFS study shows similar zirconium coordination in the initial precipitate and the digested one and excludes any strong structural perturbation on the treatment.

Table 2
Zr K-edge EXAFS fit results for the digested, nondigested and monoclinic zirconia reference

Atom	R (Å)	N	σ^2 (Å^2)	ΔE_0 (eV)
		ZR-Reflux72		
O	2.13	3.56	0.004	5.4
O	2.28	2.13	0.004	5.4
Zr	3.53	1.34	0.007	5.4
		ZR-Reflux0		
O	2.13	3.96	0.005	6.1
O	2.25	2.54	0.005	6.1
Zr	3.45	1.2	0.007	6.1
		Monoclinic zirconia reference		
O	2.11	4.5	0.005	3.2
O	2.22	2.8	0.005	3.2
Zr	3.45	5.2	0.007	3.2

3.2. Comparison of the calcined solids

Textural measurements show that silicon acts only at the calcination stage. Indeed, the noncalcined solids have the same surface area, but after calcination, the silicon-containing specimen gains advantage over its nondoped counterpart, as can be seen from Fig. 3. Therefore, silicon does not act on the stage of xerogel or humid precipitate formation, but reveals its importance only during the thermal treatment.

Dried precipitates cannot be efficiently studied by electron microscopy because they change under the microscope beam. The refluxed specimen ZR-Reflux72 was observed by HRTEM after calcination at 823 K and appeared to consist of 2- to 5-nm globules forming shapeless agglomerates (Fig. 4). After calci-

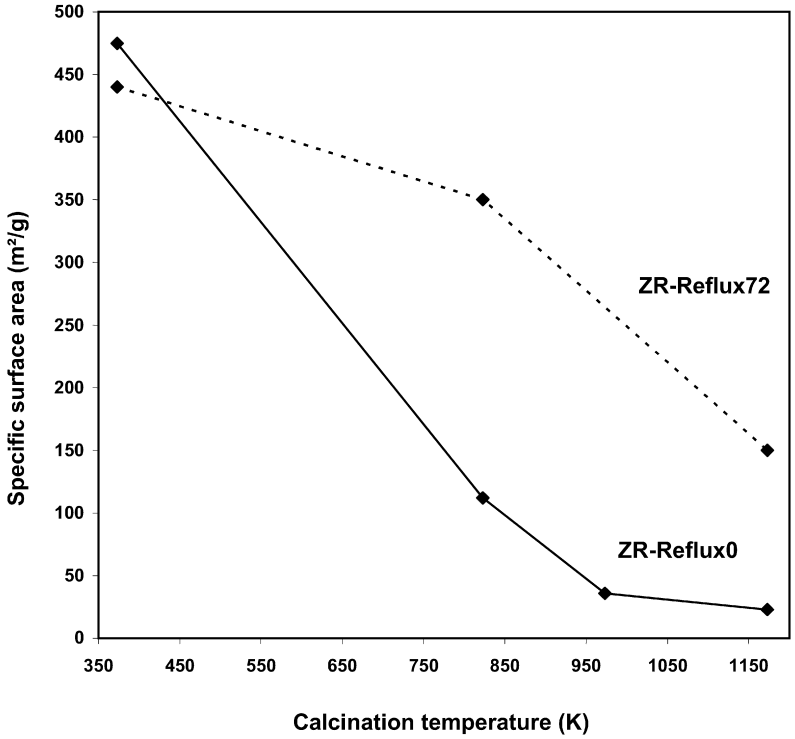

Fig. 3. Specific surface area vs calcination temperature for 4% silica-doped (ZR-Reflux72) and nondoped (ZR-Reflux0) specimens. Calcination time was 2 h.

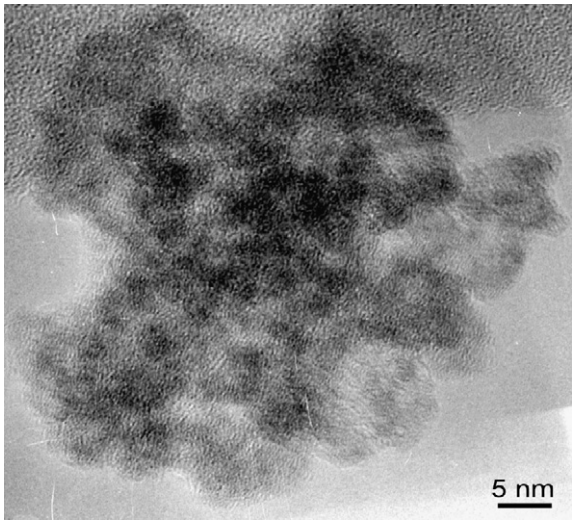

(a)

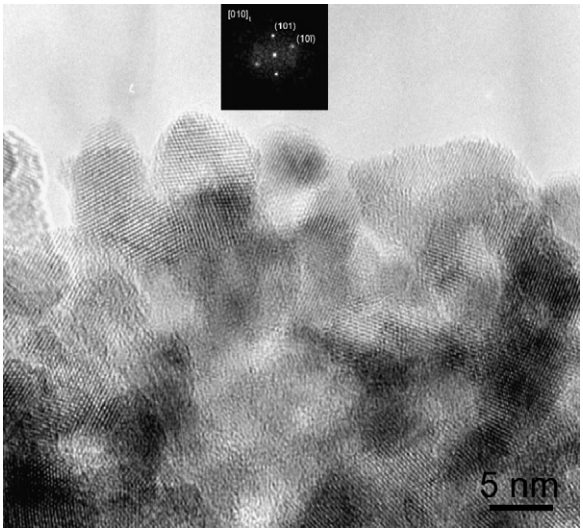

(b)

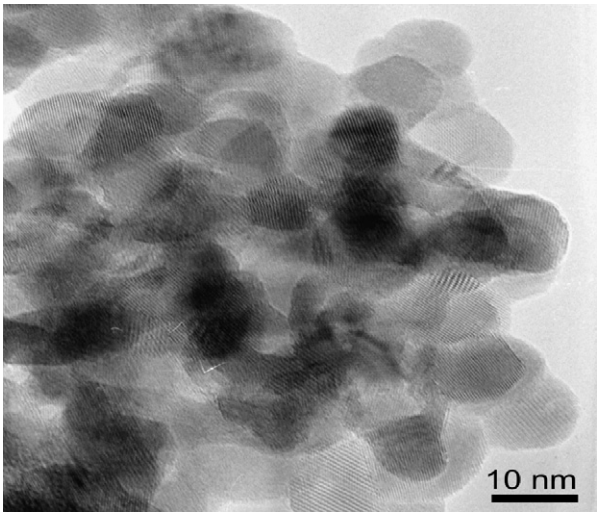

(c)

Fig. 4. HRTEM image of the amorphous precipitate ZR-Reflux72 calcined at 823 K (a); tetragonal zirconia obtained from the amorphous precipitate ZR-Reflux72 by calcination at 1173 K (b); and monoclinic zirconia obtained from the precipitate Zr-Reflux0 by calcination at 823 K (c).

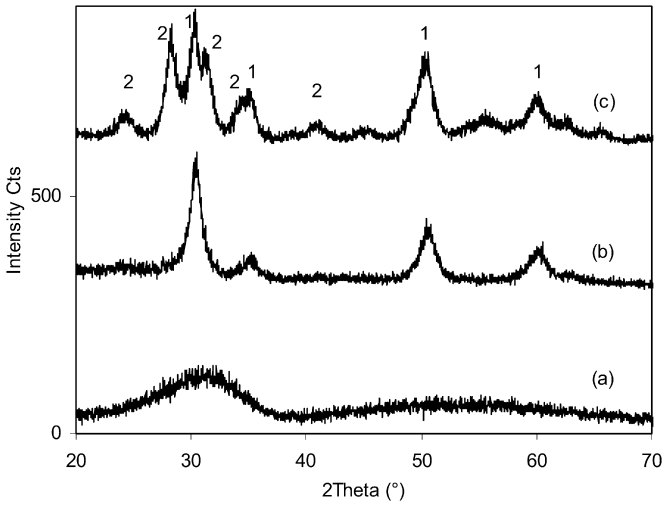

Fig. 5. XRD patterns of the solids with different silicon contents and calcined at 823 K: (a) ZR-Reflux0; (b) ZR-Reflux8; (c) ZR-Reflux72. 1—Tetragonal phase, 2—nanoclinic phase.

nation at 1173 K, this solid crystallized into 5- to 10-nm spherical particles of tetragonal zirconia (Fig. 4b). The nonrefluxed solid calcined at 823 K for 2 h showed particles of ca 10 nm with a more regular surface shape than its refluxed counterpart (Fig. 4c). It can be speculated that the silicate moieties at the surface of refluxed solid decrease the particle size; however, it is impossible to localize silicon in the solids by the HRTEM/EDX technique, because the particles are smaller than the analysis spot size (15 nm).

3.3. The state of Si in digested zirconia

Silicon-containing species, coming either from the TEOS impregnation or from the glass bulb walls, hinder zirconia crystallization and favor formation of the tetragonal variety, as demonstrated by the XRD patterns of the specimens calcined at 823 K for 2 h (Fig. 5). Such behavior has been observed earlier and was explained by stabilization of the tetragonal variety in small particles [30,31].

The stabilizing effect of silicon and improved textural properties are in agreement with earlier work, but understanding its nature requires additional characterizations. Generally, two types of T-phase-stabilizing species exist for zirconia, according to their location within the oxide particles. The first type, bulk stabilizers, include the elements of valence lower than that of zirconium (Y, Mg, Ca, La, etc.) [32–37]. They form bulk solid solutions of the second element in the zirconia network. The second group of dopants includes the oxoanions, such as sulfate, molybdate, and tungstate, which are located on the surface of the oxide particles and prevent their agglomeration [38–41]. Their mechanism of effect is related mostly to decreased surface free energy, which is a driving force of sintering [41]. In both cases, we see the tetragonal phase, but only in the second case must this tetragonal phase be highly dispersed.

Earlier it was observed that the introduction of silicon stabilizes tetragonal zirconia [42–48]. For high SiO_2 content (>30% mol), the stabilization was attributed to the constraining effect

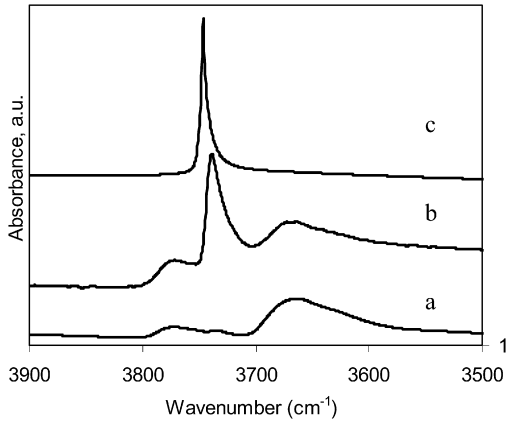

Fig. 6. OH stretching region of the IR spectra of (a) monoclinic zirconia, (b) refluxed silica doped specimen ZR-Reflux72, and (c) reference silica.

of the amorphous silica matrix on zirconia particles [42–44]. However, del Monte et al. [45,46] concluded that for content as low as 2 mol% SiO_2, silica induces decreased kinetics of zirconia grain growth. This decrease corresponds to an increase of the temperature of the tetragonal to monoclinic transformation. At higher temperatures (1473–1573 K; useless for catalysis but important for ceramics), monoclinic zirconia is formed. At the same time, silica does not crystallize but forms silica-rich glassy phase concentrates in the triple junctions of the M-ZrO_2 crystallites [47]. Such an amorphous silica-rich phase contains many substitution defects [48] and might have considerable acidity.

From the standpoint of catalysis, it seems important to know whether a stabilizing admixture belongs to the first or the second type, because the consequences for the catalytic properties of the resulting solid might be very different. Indeed, in the first case the admixture is more or less homogeneously distributed within the solid bulk and surface, and thus the surface of the support will be mostly zirconium oxide, with only small amounts of the admixture (which might, of course, be somewhat modified in its properties [33,34]). In the second case, in contrast, the surface is covered by the admixture species, especially for thermally treated solids, because the admixture moieties remain on the surface during sintering.

Because the silicon atom is small and strongly prefers tetrahedral coordination, its dissolution within the lattice of zirconia seems less probable than at the superficial location. To verify this experimentally, IR, NMR, and XPS characterizations were carried out. For the solids calcined at 823 K, IR spectroscopy revealed abundant silanol groups at 3740 cm^{-1}. These Si–OH vibrations were present as the only peak in the OH region for silica (where they are observed at 3745 cm^{-1}) and were totally absent in the spectra of the nonrefluxed monoclinic zirconia, which showed an expected doublet of lines at 3770 and 3665 cm^{-1} corresponding to isolated and bridging Zr–OH group stretching, respectively [49–51]. Analysis of peak areas suggests that for the refluxed specimen, the Si–OH moieties represent nearly half of the total OH peak area (Fig. 6). This seems to corroborate the hypothesis of strong surface enrichment by silicon, but the analysis here is only qualitative.

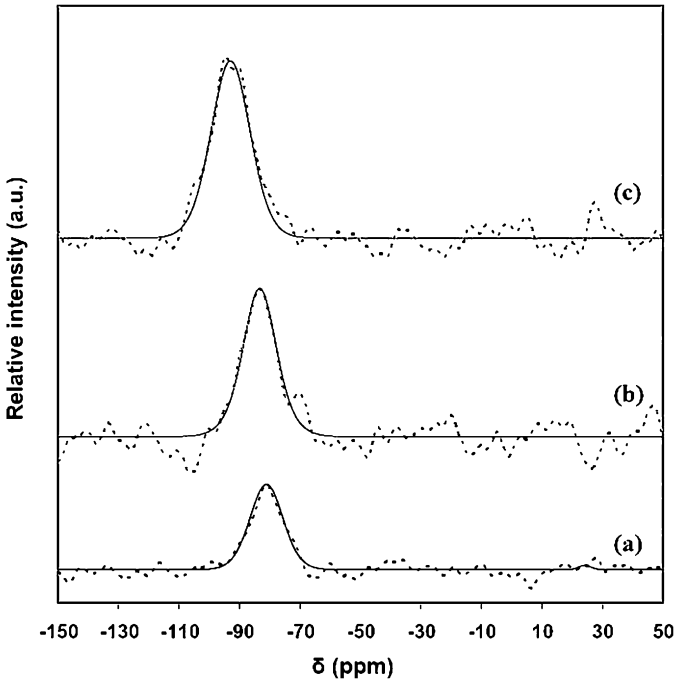

Fig. 7. ^{29}Si NMR spectra of the ZR-Reflux72 solid as a function of the calcination temperature: (a) dried at 373 K; (b) calcined at 823 K; (c) calcined at 1173 K.

Table 3
^{29}Si NMR chemical shifts for the solids studied in this work

Solid	T_{calc} (K)	δ_{Si}
ZR-Reflux72	–	−81
	823	−82
	1173	−93
ZR-TEOS-Reflux72	–	−82
ZR-TEOS-Imp	823	−84
ZR-TEOS-Coprec	823	86
SiO_2	–	−107–115[a]
$ZrSiO_4$	–	−82[a]

[a] Values extracted from Ref. [45].

The NMR signals of ^{29}Si are rather broad and noisy, due to low silicon content in the solids (Fig. 7). However, the peak positions are well defined (Table 3), and their attribution is possible. It follows from the observed chemical shifts that mainly Q^1 and Q^2 silicate species are present in the initial solids, in line with the predominance of silicate trimers and tetramers in the silicate solutions at pH 11 [52]. Unfortunately, it seems that the Si–O–Zr bond gives rise to a chemical shift similar to that of Si–O–H, and thus we cannot unambiguously determine the surface/bulk silicon location on the basis of NMR chemical shifts [53,54]. The features of the observed spectra may be summarized as follows: (i) a line centered at ca. −82 ppm always appears as a major peak in the refluxed solids; (ii) in the coprecipitated or impregnated specimens, the ^{29}Si peak is slightly shifted to the lower δ, corresponding to somewhat higher connectivity of silicon species; and (iii) calcination at high temperature again leads to a shift toward lower δ corresponding to the Q^3 species. The last transition from Q^2 to Q^3 moieties on calcination is consistent with the hypothesis of the superficial

Table 4
Si/Zr atomic ratios derived from chemical analysis and XPS data, and the intensity ratios calculated assuming a SiO_2 monolayer. The solids were prepared by basic reflux then calcined

Solid	T_{calc} (K)	S_{BET} (m^2/g)	Si/Zr, chemical analysis	Si/Zr, XPS	I_{Si}/I_{Zr}, XPS	t (nm)	β	I_{Si}/I_{Zr}, calculated[a]
ZR-Reflux72	823	350	0.18	0.26	0.03	1.0	0.14	0.03
	1173	150	0.18	0.41	0.05	2.3	0.31	0.03

[a] Si/Zr intensity ratios (last column) were calculated assuming a SiO_2 monolayer according to Kerkhof and Moulijn [55].

location of silicate groups as long as their surfaces shrink, their silicate densities increase, and they polymerize.

The XPS spectra were measured for the solids calcined at 823 and 1173 K to check the surface distribution of the elements. Core–level XPS spectra (not shown) correspond to the elements in their highest oxidation states. The binding energies provide no information on the Zr–Si interactions, because the variations in chemical shift between the corresponding binary and ternary oxides are not significant.

As follows from the data reported in Table 4, strong surface enrichment by silicon exists in the solids. For dispersed solids of small particle size (6 nm), such a strong effect requires a very strong inequality between surface and bulk composition. Note that the Si/Zr ratios from XPS cannot be interpreted as true surface atomic ratios, because both surface and bulk are "seen" by XPS for dispersed solids, although with different response factors, depending in a complex manner on the particle size distribution and the electron escape depth. In other words, for dispersed zirconia completely covered with silica monolayer, some zirconium will still be seen by XPS, but calculating its precise intensity is not possible. This does not influence the conclusion that the surface of the refluxed solid is strongly enriched with silicate species.

The ratio of XPS intensity can be estimated from the model proposed by Kerkhof and Moulijn [55]. In the case of a SiO_2 monolayer on ZrO_2, Si/Zr ratios are given by

$$\left(\frac{I_{Si}}{I_{Zr}}\right)_{XPS} = \left(\frac{n_{Si}}{n_{Zr}}\right)_{\chi} \frac{\sigma_{Si}}{\sigma_{Zr}} \frac{\beta}{2} \frac{(1+e^{-\beta})}{(1-e^{-\beta})},$$

where $(n_{Si}/n_{Zr})_{\chi}$ is the Si/Zr ratio determined by chemical analysis; σ_i is the cross-section of element i extracted from Scofield [56]; β is given by

$$\beta = \frac{t}{\lambda_{Zr}},$$

with t a characteristic thickness related to the specific area by

$$t = \frac{2}{\rho S_{BET}},$$

and λ_{Zr} is the escape depth of electrons passing through the solid. Note that kinetic energies of electrons from Si 2p and Zr 3d are not very different (1394 vs 1314 eV [57]). Thus, the difference in the escape depth of electrons from Si and Zr was neglected. Si/Zr intensity ratios calculated assuming that a SiO_2 monolayer is formed on the surface are given in Table 4.

The characterizations provide a coherent picture and indicate that the silicon species are located at the surface of the refluxed material, thus providing an exceptionally high texture-stabilizing effect. It might be interesting to compare the effect of silicon with that of molybdenum or tungsten reported earlier [41,58]. A similar mechanism likely occurs in both cases, which is not kinetically, but rather thermodynamically, controlled and is related to the formation of a metastable monolayer structure at relatively high temperatures (but below the glow phenomenon). It was observed that in molybdate-doped zirconia, molybdate species always remain on the surface, and thus when the sintering process progresses to its advanced stages, the surface area of the solid becomes proportional to the admixture content. Indeed, the surface of such a monolayer should be proportional to the amount of monolayer-forming species, either silicate or molybdate. The temperature at which this molybdenum behavior occurred was reported to be around 1073 K. Here we see again that the surface is proportional to the admixture content in a comparable temperature range (1173 K).

The silicon content for the digested solid containing 4.1 wt% Si and calcined at 1173 K was 1.42×10^{-3} mol Si per g of solid, or 9.5 μmol/m^2, corresponding to a surface content of 4–6 silicon atoms per nm^2. This value is fairly close to the "monolayer capacity" of zirconia covered by molybdate species of 5 at/nm^2 observed earlier [41]. The amount of surface occupied by one silicon atom in the calcined solids was also not far from the estimate of 0.25 nm^2 obtained for one $Si(OH)_4$ molecule [59].

The high-temperature breakthrough of monolayer with a decrease in surface area to 12 m^2/g occurred after calcination at 1473 K for 4 h. Under these rather severe conditions, monoclinic zirconia was formed, but no crystallized silica appeared. The ^{29}Si NMR spectrum of the sample showed that quasi-totality of silicon was in the Q^4 form; therefore, the silicon was not in the bulk but was in the XRD-invisible particles. The silicon likely was present in the form of amorphous bulk-like particles between zirconia crystallites, as described previously [47] for similar conditions.

It follows from our data that the surfaces of the calcined solids are covered with silicate species. In terms of catalysis or adsorption, they should behave like modified silicas rather than doped zirconias even at such a low Si content as reported here. In the next section, we evaluate this conclusion by considering three very different model reactions occurring in the presence of noble metal and sulfide active phases.

3.4. Catalytic study

The three reactions of varying nature reported here have been extensively studied; many previous papers have dealt with their mechanism, kinetics, active centers, and support effects. In all three reactions, the influence of the support is recognized as important. It was not our intent to revisit any of these reactions or the influence of support on the state of noble metal and/or sulfide active phases. We aimed only to elucidate which

Table 5
Influence of the support on the reaction rates (10^{-8} mol/(s g_{Pt})) in the presence of 1 wt% Pt supported catalysts in model reactions: hydrogenation of *ortho*-xylene (HYD); isooctane hydrocracking (HC) and the reaction rates (10^{-8} mol/(s g_{cat})) of supported (Ni)Mo sulphides activity in thiophene hydrodesulfurization (HDS)

Support	HYD[a]	HC[b]	HDS (Mo)[c]	HDS (NiMo)
γ-Al_2O_3	4.2	0.5	12	220
M-ZrO_2	7.5	1.1	24	240
SiO_2	12.3	4.0	9	171
ZR-Reflux72-Calc. 823 K	14.1	3.9	10	165
ZR-Reflux72-Calc. 1073 K	ND	ND	11	174
SiAl40	17.8	7.9	ND[d]	ND[d]

[a] HYD reaction conditions: $T = 573$ K; $P_{xyl} = 4$ kPa; flow rate of 0.45 ml/s.
[b] HC reaction conditions: $T = 523$ K; $P_{iso} = 1.7$ kPa; flow rate of 0.67 ml/s.
[c] HDS reaction conditions: $T = 573$ K; $P_{thio} = 2.4$ kPa; flow rate of 61 h^{-1}.
[d] Not determined because of rapid deactivation.

kind of support was obtained from the prolonged digestion, one with zirconia-like behavior or one with silica-like behavior.

For the platinum-supported catalysts, the reaction rates are given per gram of platinum. The platinum dispersion did not vary significantly in the catalysts studied; in hydrogen chemisorption, it varied from 0.55 for monoclinic nondigested ZrO_2 to 0.7 for digested ZrO_2, alumina, and silica supports. Thus, normalizing to dispersion would provide only a small correction without changing the reaction rates sequences. The values per exposed atom of platinum are less straightforward, because the platinum morphology is not the same on these supports, and different planes are preferentially exposed.

3.5. *O*-xylene hydrogenation

The possible products of *o*-xylene transformation are *p*- and *m*-xylenes (isomerization), toluene and trimethylbenzenes (disproportionation), and saturated C_8 naphthenes (hydrogenation). Taking into account the possibility of parallel reactions, the hydrogenating activity of hydrocracking catalysts can be characterized by the formation of alkylcyclohexanes. The isomerization of xylenes, occurring through an acid mechanism, can be used to characterize the acid activity of hydrotreating or hydrocracking catalysts [60]. The validity of *o*-xylene transformation for characterizing the acid and hydrogenating activities of bifunctional hydrocracking catalysts was confirmed in previous work [61–63].

A reversible maximum in hydrogenation activity as a function of temperature was observed at around 473 K, in agreement with the literature [61]. This was explained earlier by opposite trends of increased reaction rate and decreased surface concentration of xylene as a function of temperature.

For the Pt catalysts studied in this work, no isomerization products were observed under the reaction conditions applied. However, hydrogenating properties of platinum seem to be improved by the acidity of the support [64], and, as such, silica–alumina-supported platinum showed the best activity. The catalytic performances of platinum supported on silica-doped zirconia, obtained by digestion in basic pH, are similar to those of Pt/SiO_2 (Table 5).

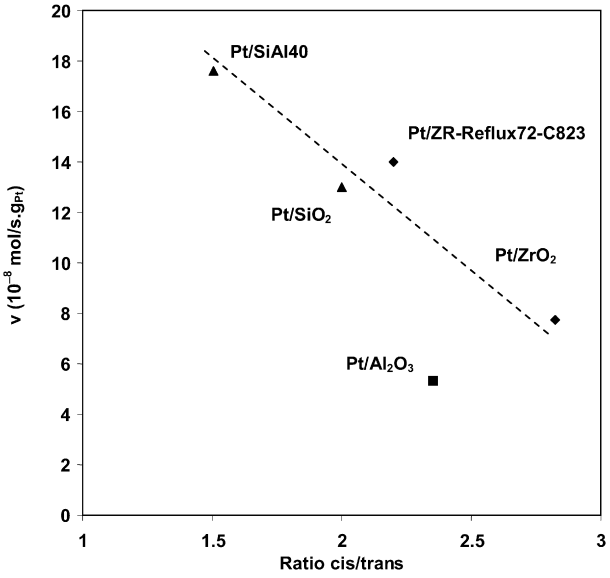

Fig. 8. Evolution of the catalytic activity vs the *cis*/*trans* dimethylcyclohexanes ratio.

Fig. 8 shows the evolution of the hydrogenation rate as a function of the ratio of both stereoisomers, *cis*- and *trans*-1,2-dimethylcyclohexane. As shown, the trans-isomer is thermodynamically more stable. Viniegra et al. [65] showed that on palladium-based catalysts, stereoselectivity to the trans-isomer was improved by increasing acidity of the support. As can be inferred from the results presented, digested zirconia supports demonstrate behavior closer to that of silica than to that of zirconia.

3.6. Isooctane hydrocracking

Isooctane HC was shown to be sensitive to the Brønsted acidity of the support, as concerns the total conversion and the selectivity of the process. Acidic supports are known to give increased amounts of cracking products. In agreement with earlier studies [25–27], the distribution of HC products is strongly dependent on the support used. The expected high reaction rate and high amount of cracking products indicated the strongest acidity of this support. At the same time, on conventional Pt/γ-Al_2O_3 or Pt/ZrO_2, mainly condensation products with 12 carbon atoms were obtained. Indeed, in our experiments, the selectivity for cracking and isomerization for the Pt/γ-Al_2O_3 and Pt/ZrO_2 catalysts was low (20 and 24%, respectively), with the remaining products due to condensation. On the other hand, digested zirconia ZR-Reflux72, silica, and silica–alumina showed 75, 72, and 85% selectivity for isomerization and cracking, respectively. Obviously, in the case of refluxed specimens, an increase in the support acidity due to silicate species at the surface favored cracking, with the production of isobutane and isobutene. Thus, both the activity and selectivity of the platinum catalysts supported on the digested solids were similar to those of silica-supported Pt.

It is noteworthy that the role of support in the HC and HYD reactions is not the same. Isooctane HC occurs on acidic centers and is aided by platinum (which helps prevent rapid cock-

ing), whereas HYD occurs on platinum and is affected by the acidity of the support. Thus, the relationship between support acidity and HYD activity is much less direct than between support activity and HC. In our tests, variations in HYD activity were smaller and less straightforwardly related to the acidity sequence.

3.7. Thiophene HDS

Strong support effects were observed for thiophene HDS in the presence of supported sulfides. The catalytic properties depend on the support acidity and the amount of available OH groups on the surface that can anchor molybdate species and further the sulfide fringes. From this standpoint, silica support was considered to give poor and unstable activity, whereas zirconia had superior intrinsic properties than standard alumina supports [1,66].

The results of HDS tests at 573 K for molybdenum- and nickel–molybdenum-supported catalysts are listed in Table 5. The relative difference between nonpromoted catalysts is great, with zirconia-supported MoS_2 being twice as active as its alumina- and silica-supported counterparts. The ZR-Reflux72 digested sample again exhibited properties similar to the silica support. MoS_2 catalysts supported on either amorphous (calcined at 873 K) or crystallized (calcined at 1073 K) solids were at the level of the silica-supported system. When promoted by nickel, the relative activity of the systems on different supports leveled off somewhat, but the sequence of activity remained the same.

The presence of silicon on the surface was probably the reason of the failed attempts to prepare highly active catalysts in our earlier studies [67]. Indeed, zirconia showed some promising properties, but when obtained with very high surface area by the digestion method, it ceased to be a good support. The reason for this obviously follows from the results of this work.

4. Conclusion

The goal of this work was to gain insight into the mechanism of zirconia textural stabilization by siliceous species during basic digestion and its implications for applications in catalysis. This work provides clear evidence that the effect is due to smearing of the siliceous species over the precipitate surface. Thus, the support surface is strongly enriched by silicon; at a Si content as low as 4 wt%, the solids show properties similar to pure silica catalytic supports for both noble metal- and sulfide-catalyzed reactions.

Acknowledgments

The authors thank C. Lorentz for carrying out the NMR measurements, P. Thérol for carrying out the XPS measurements, and the ESRF CRG committee for providing the time on the FAME beamline. Financial support for this work was provided by the Saint Gobain Company.

References

[1] M. Breysse, P. Afanasiev, C. Geantet, M. Vrinat, Catal. Today 86 (2003) 5.
[2] J. Zhu, J.G. van Ommen, A. Knoester, L. Lefferts, J. Catal. 230 (2005) 291.
[3] S. Naito, M. Tsuji, T. Miyao, Catal. Today 77 (2002) 161.
[4] Q.H. Zhang, Y. Lo, B.Q. Xu, Catal. Today 98 (2004) 601.
[5] M.K. Mishra, B. Tyagi, R.V. Jasra, Ind. Eng. Chem. Res. 42 (2003) 5727.
[6] C.N. Chervin, B.J. Clapsaddle, H.W. Chiu, A.E. Gash, J.H. Satcher Jr., S.M. Kauzlarich, Chem. Mater. 17 (2005) 3345.
[7] D.J. Suh, T.J. Park, H.Y. Han, J.C. Lim, Chem. Mater. 14 (2002) 1452.
[8] P. Afanasiev, C. Geantet, M. Lacroix, M. Breysse, J. Catal. 162 (1996) 143.
[9] P. Afanasiev, C. Geantet, M. Breysse, J. Catal. 153 (1995) 17.
[10] M.S. Wong, J.Y. Ying, Chem. Mater. 10 (1998) 2067.
[11] P. Afanasiev, A. Thiollier, M. Breysse, J.L. Dubois, Top. Catal. 8 (1999) 147.
[12] G.K. Chuah, S. Jaenicke, B.K. Pong, J. Catal. 175 (1998) 80.
[13] G.K. Chuah, S. Jaenicke, S.A. Cheong, K.S. Chan, Appl. Catal. A 145 (1996) 267.
[14] G.K. Chuah, S. Jaenicke, Appl. Catal. A 163 (1997) 261.
[15] H.L. Chang, P. Shady, W.H. Shih, Microporous Mesoporous Mater. 59 (2003) 29.
[16] S.F. Yin, B.Q. Xu, Chem. Phys. Chem. 4 (2003) 277.
[17] S.W. Wang, X.X. Huang, J.K. Guo, J. Eur. Ceram. Soc. 16 (1996) 1057.
[18] R. Rulkens, T.D. Tilley, J. Am. Chem. Soc. 120 (1998) 9959.
[19] R. Gomez, T. Lopez, F. Tzompantzi, E. Garciafigueroa, D.W. Acosta, O. Novaro, Langmuir 13 (1997) 970.
[20] J.A. Anderson, C.A. Fergusson, J. Non-Cryst. Solids 246 (1999) 177.
[21] J.A. Anderson, C. Fergusson, I. Rodríguez-Ramos, A. Guerrero-Ruiz, J. Catal. 192 (2000) 344.
[22] M. Tobo, F. Mizukami, S. Niwa, T. Sano, K. Maeda, A. Annila, V. Kommpa, J. Mol. Catal. 94 (1994) 85.
[23] J.J. Rehr, S.I. Zabinsky, R.C. Albers, Phys. Rev. Lett. 69 (1992) 3397.
[24] K.V. Klementiev, VIPER for Windows, freeware: www.desy.de/~klmn/viper.html;
K.V. Klementiev, J. Phys. D Appl. Phys. 34 (2001) 209.
[25] G. Bourdillon, C. Gueguen, M. Guisnet, Appl. Catal. 61 (1990) 123.
[26] M. Cattenot, J.L. Portefaix, J. Afonso, M. Breysse, M. Lacroix, G. Perot, J. Catal. 173 (1998) 366.
[27] M. Cattenot, E. Peeters, C. Geantet, E. Devers, J.L. Zotin, Catal. Lett. 99 (2005) 171.
[28] M.D. Rhodes, A.T. Bell, J. Catal. 233 (2005) 198.
[29] G. Aguila, S. Guerrero, F. Gracia, P. Araya, Appl. Catal. A 305 (2006) 219.
[30] R.C. Garvie, J. Phys. Chem. 69 (1965) 1238.
[31] R.C. Garvie, J. Phys. Chem. 82 (1985) 218.
[32] Y.S. Kim, C.H. Jung, J.Y. Park, J. Nucl. Mater. 209 (1994) 326.
[33] L.N. Ikryannikova, A.A. Aksenov, G.L. Markaryan, G.P. Muravieva, B.G. Kostyuk, A.N. Kharlanov, E.V. Lunina, Appl. Catal. A 210 (2001) 225.
[34] L.N. Ikryannikova, G.L. Markaryan, A.N. Kharlanov, E.V. Lunina, Appl. Surf. Sci. 207 (2003) 100.
[35] P.D.L. Mercera, J.G.V. Ommen, E.B.M. Doesburg, A.J. Burggraaf, J.R.H. Ross, Appl. Catal. 71 (1991) 363.
[36] C. Morterra, G. Cerrato, L. Ferroni, L. Montanaro, Mater. Chem. Phys. 37 (1994) 243.
[37] R. Franklin, P. Goulding, J. Haviland, R.W. Joyner, I. McAlpine, P. Moles, C. Norman, T. Nowell, Catal. Today 10 (1991) 405.
[38] K. Arata, Adv. Catal. 37 (1990) 165.
[39] P. Afanasiev, C. Geantet, M. Breysse, J. Mater. Chem. 4 (1994) 1653.
[40] C.J. Norman, P.A. Goulding, I. McAlpine, Catal. Today 20 (1994) 313.
[41] P. Afanasiev, Mater. Chem. Phys. 47 (1997) 231.
[42] V.S. Nagarajan, K.J. Rao, J. Mater. Sci. 24 (1989) 2140.
[43] T. Ono, M. Kagawa, Y. Syono, J. Mater. Sci. 20 (1985) 2483.
[44] A. Gaudon, F. Lallet, A. Boulle, A. Lecomte, B. Soulestin, R. Guinebretière, A. Dauger, J. Non-Cryst. Solids 352 (2006) 2152.
[45] F. del Monte, W. Larsen, J.D. Mackenzie, J. Am. Ceram. Soc. 83 (2000) 628.

[46] F. del Monte, W. Larsen, J.D. Mackenzie, J. Am. Ceram. Soc. 83 (2000) 1506.
[47] L. Gremillard, T. Epicier, J. Chevalier, G. Fantozzi, Acta Mater. 48 (2000) 4647.
[48] M. Nogami, J. Non-Cryst. Solids 69 (1985) 415.
[49] P.A. Agron, E.L. Fuller Jr., H.F. Holmes, J. Colloid Interface Sci. 52 (1975) 553.
[50] J.C. Lavalley, M. Bensitel, J.P. Gallas, J. Lamotte, G. Busca, V. Lorenzelli, J. Mol. Struct. 175 (1988) 453.
[51] G. Cerrato, S. Bordiga, S. Barbera, C. Morterra, Appl. Surf. Sci. 115 (1997) 53.
[52] J.W. Phair, J.S.J. van Deventer, J.D. Smith, Colloids Surf. A 182 (2001) 143.
[53] K.L. Walther, A. Wokaun, B.E. Handy, A. Baiker, J. Non-Cryst. Solids 134 (1991) 47.
[54] G. Engelhardt, D. Michel, High-Resolution Solid-State NMR of Silicates and Zeolites, Wiley, New York, 1987, p. 75.
[55] F.P.J.M. Kerkhof, J.A. Moulijn, J. Phys. Chem. 83 (1979) 1612.
[56] J.H. Scofield, J. Electron Spectrosc. Relat. Phenom. 8 (1976) 129.
[57] C.D. Wagner, W.M. Riggs, L.E. Davis, J.F. Moulder, G.E. Muilenberg, Handbook of X-Ray Photoelectron Spectroscopy, Perkin-Elmer Corp., Eden Prairie, MN, 1992.
[58] J.R. Sohn, M.Y. Park, Langmuir 14 (1998) 6140.
[59] K.I. Marinakis, H.L. Shergold, Int. J. Miner. Process. 14 (1985) 177.
[60] D. Zuo, M. Vrinat, H. Nie, F. Maugé, Y. Shi, M. Lacroix, D. Li, Catal. Today 93–95 (2004) 751.
[61] A. Kalantar Neyestanaki, H. Backman, P. Mäki-Arvela, J. Wärna, T. Salmi, D.Yu. Murzin, Chem. Eng. J. 91 (2003) 271.
[62] H. Backman, A. Kalantar Neyestanaki, D.Yu. Murzin, J. Catal. 233 (2005) 109.
[63] S. Smeds, D. Murzin, T. Salmi, Appl. Catal. A 150 (1997) 115.
[64] S.D. Lin, M.A. Vannice, J. Catal. 143 (1993) 359.
[65] M. Viniegra, G. Cordoba, R. Gomez, J. Mol. Catal. 58 (1990) 107.
[66] M. Breysse, J.L. Portefaix, M. Vrinat, Catal. Today 10 (1991) 489.
[67] M. Jia, P. Afanasiev, M. Vrinat, Appl. Catal. A 278 (2005) 213.